Temperature and Pressure Dependence of the AMOEBA Water Model

Pengyu Ren and Jay W. Ponder*

Department of Biochemistry and Molecular Biophysics, Washington University School of Medicine, St. Louis, Missouri 63110

The temperature and pressure dependence of the previously developed polarizable atomic-multipole-based AMOEBA water potential is explored. The energetic, structural, and dynamical properties of liquid water are investigated via molecular dynamics simulations at various temperatures ranging from 248 K to 360 K and pressures up to 5000 atm. The AMOEBA model, derived solely from known gas-phase and room-temperature liquid properties, produces a maximum liquid density around 290 K at 1 atm. The quantitative agreement between AMOEBA and experiment is good in general for density, heat of vaporization, radial distribution functions, magnetic shielding, self-diffusion, and static dielectric constant. Based on comparison of two variants of AMOEBA water, as well as results from other water potentials, it is suggested that the temperature at which the maximum density occurs is closely related to the tetrahedral hydrogen-bonding network in the bulk. Explicit dipole polarization and internal geometry in the liquid play vital roles in determining the self-diffusion and dielectric constants. The development of the AMOEBA model demonstrates that a realistic and well-balanced atomic potential requires a sophisticated electrostatic description and inclusion of many-body polarization. Within the current polarizable atomic multipole framework, a potential derived from limited gas phase and condensed phase properties can be applied across a range of physical and thermodynamic environments.

Introduction

Modeling of electronic polarization and other effects such as proton dissociation were introduced into empirical water potentials over two decades ago.[1-3] However, it is only in the past several years that systematic attempts have been made to implement such models for use in general simulations of substances other than water. In the search for more accurate potentials, increasing effort has been devoted to improving the electrostatic description via inclusion of lone-pair charge sites, higher-order electrostatic moments, and secondary effects such as electronic polarization. The main advantage of polarizable models is their ability to adapt spontaneously to changes in the physical-chemical environment. Examples include changes from a vapor to a liquid phase, from a polar to a nonpolar milieu, and from a neutral to a highly charged environment as often observed in biological systems. This adaptability is critical for modeling the coexistence of multiple phases of water, whose dipole moment is enhanced by nearly 50% upon moving from gas phase to the liquid. Furthermore, polarization also enhances the transferability of a general potential model that aims to describe interactions in heterogeneous molecular systems, where nonideality is a direct result of many-body effects.

Even though most water potentials have been derived for and applied to ambient conditions, many chemical and biological processes require water to undergo temperature or pressure changes. As a result, nonpolarizable force fields face the dilemma of having to describe a wide range of conditions with a single set of parameters. Due to their implicit inclusion of polarization, models with fixed electrostatics can only rely on one specific environment for their parametrization. Consequently the determination of unambiguous parameters for different energy components (e.g., electrostatics and repulsion-dispersion) becomes problematic. Explicitly polarizable water models have the potential to reduce this concern.

Among the nearly 50 water models reviewed by Gulliot[4] in 2002, almost half are polarizable. The number is apparently still growing; for example, two Drude oscillator-based polarizable force fields, the charge-on-spring (COS) model[5] and the SWM4-DP model,[6] have recently been published. Some of the other recent water potentials, including BSV,[7,8] POL5/TZ(QZ),[9] PPC,[10] TIP4P/FQ,[11] and TIP5P[12] have been applied with reasonable success to study of the temperature or pressure dependence of water properties. Of these, only TIP5P does not include explicit polarization. Results with TIP5P indicate that polarization may not be necessary to reproduce many water properties, and its enhanced electrostatic description due to introduction of additional charge sites evidently improves its performance. However, the parametrization of TIP5P involved direct fitting to experimental temperature dependence data. The predictive power of such a model is limited, and it would be prohibitive to exploit this approach in parametrization of a general force field. The other polarizable models seem to enjoy a similar degree of success to TIP5P, especially in terms of reproducing the temperature of maximum density (TMD). However, problems still exist with all current models. The BSV model[7] gives rise to too steep of a decrease in density at temperatures above the TMD. Similar to TIP5P, the polarizable PPC[10] model displays a sharp transition in its density through the TMD region, even though other thermodynamic properties calculated at fixed experimental density show good agreement with experiment. The PPC potential appears to be "under polarized" as it exhibits a gas-phase dipole moment (2.14 D) between the true gas-phase value (1.85 D) and estimates of the

* Corresponding Author: Tel: (314) 362-4195. Fax: (314) 362-7183. E-mail: ponder@dasher.wustl.edu.

condensed phase value (>2.6 D). In addition, the PPC model has zero polarizability in the out-of-plane direction, while the experimental polarizability in this direction (1.4 Å^3) is almost as large as in orthogonal directions. The authors state that attempts to parametrize a fully polarizable model resulted in degradation of computed liquid properties. The POL5/TZ(QZ) potential[9] is a true ab initio model, like our AMOEBA (Atomic Multipole Optimized Energetics for Biomolecular Applications) model,[13] in the sense that the gas-phase molecular dipole and quadrupole moments, and cluster binding energies for the dimer through hexamer, are comparable to high-level ab initio results, while experimental liquid properties are also reproduced. A major difference between AMOEBA and POL5 is that our model adopts ab initio-derived atom-centered multiple moments through the quadrupole, and avoids the use of underdetermined off-atom charge sites. In addition, AMOEBA accounts for polarization via induced dipole moments rather than fluctuating charges.

Explicit polarization provides a physical means for separating the different contributions to molecular interactions. It allows direct utilization of high-level ab initio calculations in the gas phase for derivation of the permanent electrostatic moments, making such models attractive in deriving general force fields. The many-body effects should be verified via comparison with ab initio energies and structures of various small clusters. Once an independent electrostatic model is finalized, limited liquid properties can be used to refine the vdW (repulsion-dispersion) parameters, which are not well-determined by cluster properties. This is a somewhat simplified picture, and polarization is not the only physical element missing from the current generation of classical pairwise models. Nonetheless, direct treatment of polarization is the most important remaining step toward more realistic potentials for general molecular simulation.

Using the above approach, we are developing a complete polarizable atomic multipole-based force field for biological studies. As the first step toward this goal, an AMOEBA water model was reported in an earlier publication.[13] This model was derived from ab initio data and ambient liquid density and heat of vaporization, and validated for a spectrum of gas-phase and condensed-phase properties. In the present work, the model is applied, without any further modification, to simulate liquid water over a wide range of temperatures above and below the freezing point, and at a series of high pressures. Comparison is made against other recently developed water potentials, as well as a variant of the AMOEBA model. Contrasting the success and failure of different polarizable and nonpolarizable models over a range of thermodynamic conditions furthers our understanding of the physical chemistry of water at the microscopic level, but also provides an insight into the development of transferable atomic potentials for other molecules. It is our goal in the following sections to demonstrate that the AMOEBA model behaves satisfactorily over a range of temperature and pressure conditions. Equally important, parametrization of the model is robust in the sense that extension to other molecular systems is straightforward.

Computational Details

The details of the AMOEBA water model and its parameters have been described previously.[13] Molecular mechanics calculations were carried out using the TINKER molecular modeling package.[14] A cubic box of either 216 or 512 water molecules was used to compute all properties, other than the dielectric constant (which is discussed below). For the temperature

dependence at 1 atm pressure, results from both the 216- and 512-molecule systems were obtained, while pressure-dependence studies were carried out on boxes of 216 water molecules. Periodic boundary conditions were imposed throughout, with long-range electrostatic interactions treated using the standard Ewald summation technique. All molecular dynamics production simulations used a 1 fs time step. Sample calculations at 298 K and 1 atm were performed using a 0.1-fs time step, yielding identical results within statistical error for the thermodynamic properties studied here. A tapering function based on a 1.2-Å switching window is used to reduce vdw interactions to zero at distances beyond 12 Å. The Berendsen thermostat and barostat[15] were used to enforce constant temperature and pressure. Note that the Berendsen weak-coupling methods do not correspond to any standard ensemble, but Morishita[16] has derived formulae for computing fluctuation properties from the ensemble associated with weak-coupling. Simulations of the 512-molecule box between 255 K and 360 K were carried out for 1.5 ns at temperatures of 290 K and below, 1 ns at 298 K, and 700 ps above 298 K. To sample the density of the smaller 216 molecule box, similar simulations were carried out for various lengths ranging from 1 to 3 ns. The first 200 ps of each MD trajectory were deemed the equilibration period, and this portion was discarded when computing average properties. The heat of vaporization, ΔH_v, at 273 K and above was calculated from constant pressure simulations, rather than at fixed experimental density, using

$$\Delta H_v = H_{gas} - H_{liq} \approx U_{gas} - U_{liq} + RT \qquad (1)$$

where H is the enthalpy and U is the potential energy in kcal per mole of molecules. The kinetic energy contributions in the gas and liquid phases essentially cancel, and the PV term for the liquid is negligible relative to the corresponding term (RT) for the gas phase. An analytical formula consisting of a 5th degree polynomial was fitted to the temperature dependence of the enthalpy H of liquid water at 1 atm. Differentiation of this formula gives a relation for the heat capacity:

$$C_P = \left(\frac{\partial \langle H_{liq} \rangle}{\partial T}\right)_P \qquad (2)$$

Substituting $\langle H \rangle = \langle U \rangle + \langle K \rangle + \langle PV \rangle$ into this equation results in

$$C_P = \left(\frac{\partial \langle U_{liq} \rangle}{\partial T}\right)_P + \frac{9}{2}R \qquad (3)$$

where $\langle K \rangle$ is the internal kinetic energy, and each degree of freedom contributes $R/2$ to the heat capacity. Note that eq 3 is for a flexible water model, where there are nine degrees of freedom per molecule. For a rigid model, the second term in eq 3 is reduced to 3R. The $\langle PV \rangle$ term for the liquid is assumed to be independent of temperature within the range studied.

Water−dimer interaction energies are computed with respect to the flap angle, τ in Figure 7, in the following fashion. First, the dimer is optimized for each potential. Then, with the internal geometry of each molecule fixed, the flap angle is changed by rotating the hydrogen bond acceptor molecule while the molecular planes are kept perpendicular to each other as in the dimer minimum. Ab initio energies as a function of flap angle are obtained at the LMP2/aug-cc-pVQZ level using the Jaguar program.[17]

AMOEBA Water Model

J. Phys. Chem. B, Vol. 108, No. 35, 2004 **13429**

The water self-diffusion coefficients were evaluated from the mean-square-displacement (MSD) using the Einstein relation,

$$D = \frac{1}{6}\lim_{t \to \infty}\frac{d}{dt}\langle|\underline{r}(t) - \underline{r}(t_0)|^2\rangle \qquad (4)$$

The static dielectric constant was estimated from droplet simulations, where a water sphere of radius 12 Å containing 242 molecules was retained inside a wall boundary potential as described previously.[13] The fluctuation of the droplet dipole moment sampled from a nonperiodic constant temperature simulation is related to the static dielectric constant by[18]

$$\frac{\langle M^2\rangle}{k_B T r_1^3} = \frac{(\epsilon_1 - 1)[(1 + 2\epsilon_2)(2 + \epsilon_2) - 2(r_1/r_2)^3(1 - \epsilon_2)^2]}{(\epsilon_1 + 2\epsilon_2)(2 + \epsilon_2) - 2(r_1/r_2)^3(1 - \epsilon_2)(\epsilon_1 - \epsilon_2)} \qquad (5)$$

where r_1 and r_2 are the radii of the inner and outer shells respectively, and M is the total dipole moment of the inner sphere. All nonbonded interactions within the droplet were computed without cutoffs, and radii of $r_1 = 6$ Å and $r_2 = 12$ Å were used. The dielectric constant of the inner shell, ϵ_1, can be determined from the equation by either setting $\epsilon_2 = 80$ or invoking the approximation $\epsilon_1 \approx \epsilon_2$. Our previous calculations showed that the results obtained from a periodic simulation using Ewald summation ($\epsilon = 82$) and a droplet simulation ($\epsilon = 81$) are in close agreement at ambient temperature and pressure. Due to the cost of traditional Ewald simulation, we have chosen to use droplet simulations at a series of selected temperatures to compute dielectric constants. Simulations of 2 ns were carried out for temperatures of 323 K and below, while 1 ns was found to be sufficient at higher temperatures. The statistical error of the simulation results are estimated by the same method described in our previous AMOEBA water study.[13]

Results and Discussion

Density. It is well-known that the density of liquid water exhibits anomalous temperature dependence. The maximum density under 1 atm of pressure, 0.99995 g/cm³, occurs at 277 K. A number of water models, including BSV,[7,8] PPC,[10] TIP4P/FQ,[11] and TIP5P[12] are reported to reproduce the temperature of maximum density within a few degrees. Other models, such as COS,[5] NEMO,[19] SPC,[20] and TIP3P,[21] display no TMD within the commonly studied temperature range. Still other potentials, SPC/E,[22] ST2,[23] TIP4P,[21] POL5/TZ, and POL5/QZ,[9] have well-defined TMDs that deviate from 277 K to various extents. However, among models that precisely replicate the TMD, none accurately reproduces water density at temperatures away from the TMD, and their deviation from actual densities increases as the temperature moves further from the TMD. TIP5P, for which densities over a range of 150 K have been reported, shows too strong of a temperature dependence (i.e., the computed density becomes too low) above 277 K. The density of polarizable PPC, reported between 267 K and 298 K,[17] exhibits a very similar trend. Densities calculated with the BSV model decrease even more quickly as the temperature increases above 280 K.

Due to the large number of water potentials in the literature, it is prohibitive to discuss all of them in detail. Instead, we will focus on recently developed potentials and mention older models only as necessary. The density of water as a function of temperature calculated with selected water models is compared with experimental measurements[24] in Figure 1. It is immediately clear that all theoretical models exhibit a sharper density
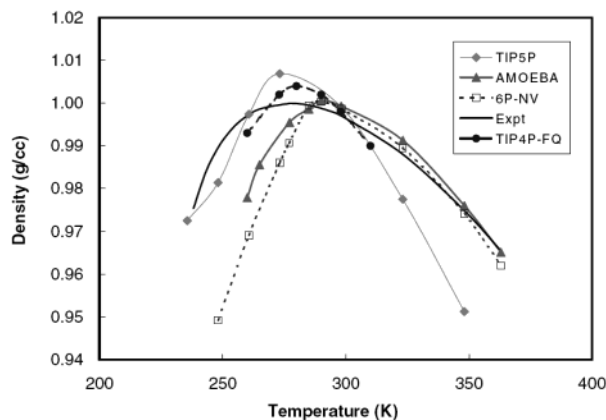

Figure 1. Temperature dependence of the density of water at 1 atm pressure. The experimental data are from Kell.[24]
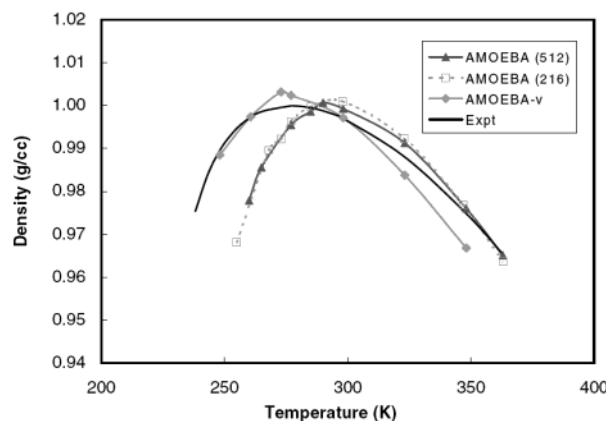

Figure 2. Temperature and system-size dependence of the density of AMOEBA and AMOEBA-v water. The experimental data are from Kell.[24]

transition than real water. The TIP5P results shown are those reported by Mahoney and Jorgensen[12] from Monte Carlo simulations with molecule-based truncation of nonbonded interactions at 9 Å. A related rigid, fixed-charge water model included in the comparison is an extension of TIP5P to a six-site model as proposed recently by Nada and van der Werden.[25] This potential is represented as 6P−NV in the following discussion. Both TIP5P and 6P−NV have been explicitly parametrized to reproduce the temperature dependence of water properties. The main differences between the TIP5P and 6P−NV models are that the latter has a longer OH bond and a larger HOH angle, hydrogen vdW sites, and an extra charge site located near the molecular center-of-mass. The TIP4P−FQ potential[11] is a polarizable model with fixed geometry taken directly from the original TIP4P model. POL5/TZ and POL5/QZ[9] are two recently developed rigid five-site models that combined fluctuating charges and induced dipoles in their treatment of polarization, These models closely resemble TIP4P−FQ in the shape of their temperature vs density curves, but have the TMD shifted to about 295 K with the entire curve shifted to lower density by approximately 0.01 g/cm³.

The TIP5P and AMOEBA results shown in Figure 1 are obtained from simulations on boxes of 512 molecules. It was previously reported that the TMD for TIP5P increased from 280 K to 295 K when either a smaller box of 216 molecules or a smaller cutoff for charge interactions was used. When Ewald summation is used for AMOEBA, we find the density−temperature curves for 512- and 216-molecule systems to be identical within statistical accuracy, as shown in Figure 2. This result suggests the finite-size dependence in TIP5P simulations

may have been due to the differing electrostatic cutoff methodologies. The maximum density of the AMOBEA water model occurs at approximately 290 K, as is also the case for the 6P−NV model. This temperature is closer to the TMD of D_2O, 285 K, than to that of ordinary water. In addition, AMOEBA water displays a somewhat broader density transition than the rigid TIP5P, 6P−NV, and TIP4P/FQ models, even though the AMOEBA curve is still narrower than experiment. The agreement between AMOEBA and experiment is excellent above 273 K, whereas the AMOEBA density in the supercooled region decreases too steeply at cooler temperatures. The statistical uncertainty (standard error) of the sampled density is 0.0051 g/cm^3 at 255 K and 0.0001 g/cm^3 at 363 K, with generally smaller uncertainty at the higher temperatures in this range.

In previous studies, Jorgensen and Jenson[26] have investigated the temperature dependence of the density for the fixed charge SPC, TIP3P, and TIP4P water models. Neither of the three-site SPC and TIP3P models produced a maximum between 323 K and 473 K, and their densities increased monotonically with decreasing temperature. However, the TIP4P potential does have a density maximum of 1.018 g/cm^3 at 260 K. The parametrization of TIP5P revealed that the temperature dependence of its density is very sensitive to the position of lone pairs on the oxygen atom, and tuning this position allows accurate reproduction of the correct TMD of water. By contrast, no information on temperature dependence was used in the parametrization of AMOEBA, and no adjustment of electrostatic parameters was made when computing the density profile.

Furthermore, AMOEBA is a flexible model that allows internal geometry changes. Interestingly, the water geometry is found to have a strong influence on the anomalous density maximum. To illustrate this point, we present in Figure 2 results from a variation of our AMOEBA model (abbreviated as AMEOBA-v) that was previously investigated in the process of obtaining the final AMOEBA potential. The major difference between AMOEBA-v and AMOEBA lies in the choice for the equilibrium HOH bond angle. Other parameters were optimized following identical protocols, so the vdWs and electrostatic parameters vary insignificantly. The hydrogen reduction factor is changed from 0.85 to 0.91 solely because the latter provides a superior fit to water dimer structures and energies of configurations other than the equilibrium structure.[13] The detailed force field parameters for AMOEBA and AMOEBA-v are compared in Table 1. The latter model has a TMD around 275 K, and the density in the supercooled region is in excellent agreement with experiment. To illustrate the difference between the two models, the molecular moments computed by each are listed in Table 2. As previously discussed,[13] the flexible AMOEBA model adopts a larger equilibrium angle of 108.5° in the gas phase such that the average angle in the condensed liquid-phase becomes 105.3°, in good agreement with experimental and QM simulation evidence. AMOEBA-v has a "correct" equilibrium HOH angle of 104.5° in the gas phase, which contracts to 101° in liquid water. We have previously discussed the hypothesis that unphysical contraction of the HOH angle is a consequence of the lack of geometric dependence of electrostatics in AMOEBA; that is, the permanent atomic multipoles of water remain constant with respect to bond stretching and angle bending. Approaches to incorporate such effects have been suggested.[27] Furthermore, the AMOEBA HOH angle expands slightly in the liquid from 105.12° to 105.60° as the temperature rises from 255 K to 348 K. This trend contradicts a theoretical estimate of the perturbation in liquid water that suggests a small angle contraction with rising

TABLE 1: Parameters for the AMOEBA and AMOEBA-v Water Models

		AMOEBA	AMOEBA-v
O−H Bond	b_0 (Å)	0.9572	0.9572
	K_b (kcal/mol/Å^2)	529.6	529.6
H−O−H angle	θ_0 (deg)	108.50	104.52
	K_θ (kcal/mol/rad^2)	34.05	34.05
Urey−Bradley	l_0 (Å)	1.5537	1.5139
	K_1 (kcal/mol/Å^2)	38.25	38.25
van der Waals			
O	R_0 (Å)	3.405	3.410
	ϵ (kcal/mol)	0.110	0.114
H	R_0 (Å)	2.655	2.820
	ϵ (kcal/mol)	0.0135	0.0160
	reduction[a]	91%	85%
polarizability	α (Å^3)		
O		0.837	0.837
H		0.496	0.496
multipoles			
O	q	−0.51966	−0.51966
	d_z	0.14279	0.14279
	Q_{xx}	0.37928	0.33928
	Q_{yy}	−0.41809	−0.41809
	Q_{zz}	0.03881	0.07881
H	q	0.25983	0.25983
	d_x	−0.03859	−0.03859
	d_z	−0.05818	−0.05818
	Q_{xx}	−0.03522	−0.03673
	Q_{yy}	−0.10298	−0.10739
	Q_{zz}	0.13820	0.14412

[a] The Reduction Factor defines the position of the hydrogen vdW center as a percentage of the distance from O to H along their internuclear vector.

TABLE 2: Dipole and Quadrupole Moments of Water

	Expt	**AMOEBA**[c]	AMOEBA-v
μ	1.85[a]	1.77 (1.85)	1.85
Q_{xx}	2.63[b]	2.50 (2.35)	2.30
Q_{yy}	−2.50[b]	−2.17 (−2.16)	−2.16
Q_{zz}	−0.13[b]	−0.33 (−0.20)	−0.14

[a] Clough et al.[52] [b] Verhoeven and Dymanus.[53] [c] AMOEBA values are for the ideal bond angle of 108.5°, values in parentheses are for the experimental gas-phase angle of 104.52°.

temperature.[28] The only available experimental neutron diffraction data show no overall tendency between 298 K and 473 K.[29] Even though the DOD angle derived from OD and DD distances increases from 106.56° at 298 K to 107.35° at 323 K, all other data points at higher temperatures fluctuate insignificantly around the former value. Subtle changes in water geometry with temperature, especially the HOH angle, may play an important role in the water density anomaly. It is conceivable that models with geometry-dependent electrostatics can produce the correct geometric response to changes in temperature, as well as the transition from gas to liquid.

Additional evidence for the influence of the bond angle on the density profile is revealed by a comparison between TIP5P and 6P−NV. One goal in the creation of the 6P−NV model from TIP5P was to reproduce the experimental melting free energy of ice.[25] Interestingly, the 6P−NV model uses a fixed HOH angle of 108°, and has a density vs temperature curve similar in shape to that of TIP5P with its fixed HOH angle of 104.5°. However the 6P−NV curve is shifted to higher temperature and lower density, resulting in a good agreement with the AMOEBA results.

The development of the TIPxP series of potentials points to an intrinsic dilemma for nonpolarizable models: the parameters determined from ambient liquid phase properties are not unique, and some choices will perform poorly under other conditions.
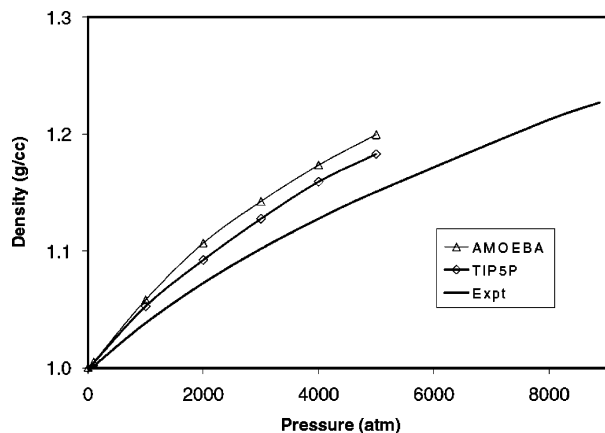
AMOEBA Water Model

J. Phys. Chem. B, Vol. 108, No. 35, 2004 **13431**

Figure 3. Pressure dependence of water density at 298 K. The experimental data are from Sato et al.[30]

Figure 4. Temperature dependence of the AMOEBA water O···O RDF at 1 atm pressure.

For example, the addition of off-atom sites in moving from TIP3P to TIP4P to TIP5P generally improves the electrostatic treatment. However, none of the TIPxP models appears to provide the correct average molecular moments in the liquid. The density vs temperature dependence of the various models further demonstrates the need for a nonpolarizable model to fit as many liquid properties as possible in order to provide an "averaged" electrostatic description for the condensed phase. In contrast, a polarizable model such as AMOEBA is subject to less ambiguity since it can rely on high level ab initio calculations to determine permanent electrostatic parameters. However, empirical optimization is still required to determine the vdW parameters. Using either experimental or ab initio polarizabilities, the vdW values can be derived to maintain consistency between gas-phase clusters and liquid simulations. The resulting potential energy is well balanced, and as evident from the above simulations, can be reasonably applied under different conditions without further modification.

The pressure dependence of density for AMOEBA water at 298 K has also been investigated. The density sampled from MD simulation was typically well-equilibrated within 200 ps. Following equilibration, an additional 300 ps of trajectory was generated and analyzed to obtain converged values at the various pressures. The standard errors are within ± 0.0005 g/cm^3. The results are compared with experimental densities[30] and those reported for TIP5P[12] in Figure 3. The isothermal compressibility at room temperature, estimated from the slope of the curve at 1 atm, is roughly 55×10^6 atm^{-1}. This is higher than the experimental value of 45.8×10^6 atm^{-1}, but lower than values reported for TIP3P and TIP4P. Even though the density profile of TIP5P is very similar to that of AMOEBA in the low-pressure region, a lower value of 41×10^6 atm^{-1} for TIP5P was obtained by Mahoney and Jorgensen.[12] The TIP5P model, which uses a Lennard−Jones 12−6 vdW potential, is more compressible than real water at high pressure. The buffered 14−7 vdW potential used with AMOEBA, which is softer than Lennard−Jones in the short-range repulsive region, leads to an even higher compressibility. This seems to contradict the commonly held view that Lennard−Jones potentials have too stiff of a repulsive wall based on comparison with experimental rare gas potentials.[31] Furthermore, the compressibility of both AMOEBA and TIP5P, related to the slopes of their density vs pressure curves, are more problematic within the 1 to 2000 atm range than at higher pressures. The too-high absolute density at high pressure is merely the result of a high compressibility at relative low pressure. In fact, the density vs pressure slope actually approaches that observed in experiment for pressures above 3000
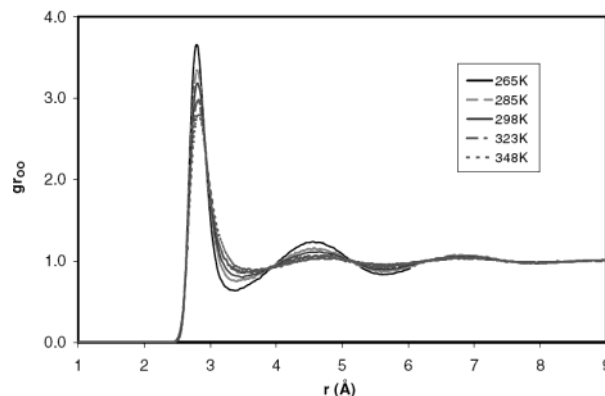
bar, indicating saturation of the ability to undergo compression. It is conceivable that an alternative functional form for vdW interactions, rather than reparametrization of existing models, will be required to improve the compressibility of water models.

Radial Distribution Functions. The radial distribution functions (RDF) of liquid water provide information about the average packing of molecules, and can be derived from experiments such as neutron[32] and X-ray[33] scattering. Figure 4 summarizes the O···O RDF of AMOEBA water as sampled from simulations of a 512-molecule box at temperatures from 265 to 363 K and 1 atm of pressure. Clearly, the first peak height is reduced as temperature increases, but the position of the first peak remains nearly constant. Another apparent change is that the first minimum and the second peak become less pronounced with increasing temperature. The effect of pressure is not shown, but is very similar to that of increasing temperature. The major difference is that increasing pressure insignificantly alters the first peak height. For example, at a pressure of 3000 atm, the height of the first peak is only reduced by 0.2 vs the 1 atm value, even though features beyond the first peak are already flattened and beginning to disappear. This picture is consistent with the current state-of-the-art theory that water is a dynamic, rapidly changing mixture of tetrahedral ice Ih-like and denser ice II-like structures.[34] The nearest neighbors are well-defined in both types of ice with an O···O separation of about 2.8 Å. However, the next-nearest neighbor O···O distance is about 4.5 Å in the tetrahedral ice Ih structure, and only 3.4 Å in ice II. The former distance corresponds to the usual location of the second peak in the O···O RDF, while the latter distance correlates with the location of the first minimum. As the temperature rises, the amount of ice II-like structure grows, whereas the ice Ih type of tetrahedral structure becomes less populated, leading to a flattening of the RDF beyond the first peak. A possible rationalization is that the ice Ih structure is favored by the hydrogen-bonding interactions within the tetrahedral arrangement, while dispersion forces are predominant in ice II.[34] Transforming from the former to the latter would require energy to bend the hydrogen bonds while gaining favorable dispersion interactions. Within this framework, the water density maximum can be interpreted as the result of a competition between the typical thermal contraction and the rising proportion of less-dense ice Ih-like structures at lower temperature.

As noted above, the AMOEBA and AMOEBA-v force field parameters differ only slightly, yet their TMDs are separated by about 15 K. Hence, it is of interest to compare the RDFs of these two models at various temperatures. Figure 5 shows the change in the RDF of AMOEBA-v from 298 K to 260 K is
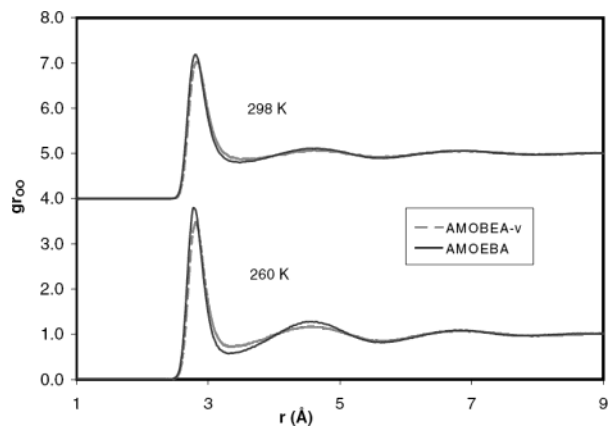
Figure 5. Comparison of the AMOEBA and AMOEBA-v water O···O RDFs at selected temperatures.
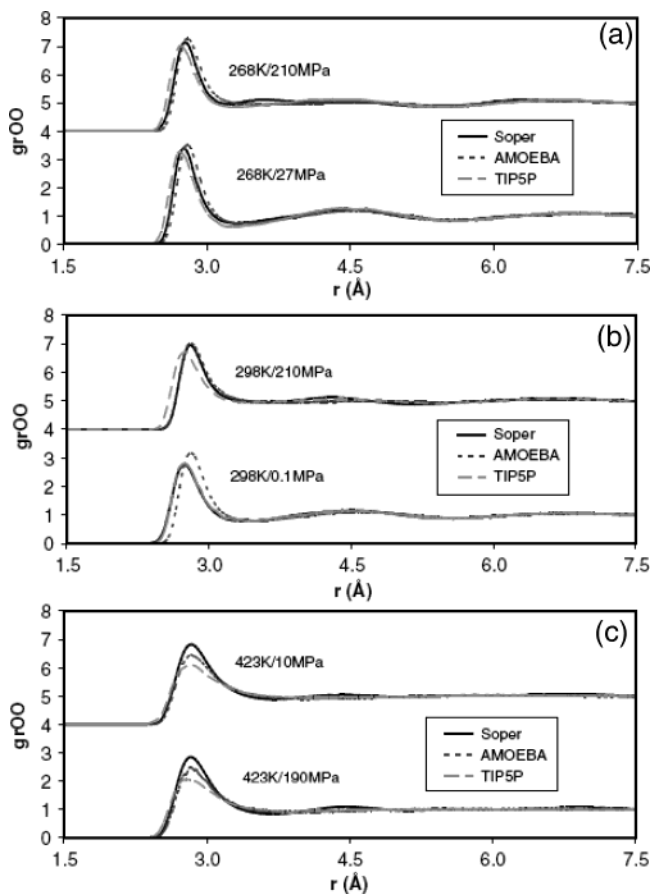

Figure 6. Comparison of experimental and simulated O···O RDFs at various temperature−pressure conditions. The experimental data are from Soper.[35]

Figure 7. Potential energy of the water dimer as a function of the flap angle, τ.

AMOEBA and TIP5P RDFs remain nearly invariant throughout the full temperature and pressure range. However, the experimental first peak location exhibits stronger pressure dependence at room temperature than does either set of simulations. At 298 K the experimental first peak shifts from agreement with the TIP5P position to agreement with AMOEBA as the pressure is increased from 0.1 to 210 MPa. At lower or higher temperatures, the AMOEBA RDFs show very good agreement with those of Soper for the first peak locations, which are rather insensitive to the high pressure. It is not clear if the strong pressure dependence at room temperature is an artifact of the neutron-scattering data analysis or a special characteristic of water at room temperature that empirical potentials are unable to reproduce. At the elevated temperature of 423 K, the first peak in the AMOEBA RDF is too low in comparison with the RDF derived from neutron scattering, while the TIP5P peak is even lower. This is reflected in the low density of TIP5P water at this high temperature as suggested by the trend in Figure 1. At all temperatures, pressure effects on the RDF, especially features beyond the first peak, seem to correlate with the overestimation of isothermal compressibility by AMOEBA and TIP5P. According to the two-state theory described above, the RDF between 3 and 5 Å becomes flat at high pressure as tetrahedral local structures are replaced by ice II-like states.

The agreement between the AMOEBA and experimental O···H RDFs is similar in quality to that for the O···O RDFs (not shown). The main exception is that at 423 K the O···H RDFs from the AMOEBA model compare very well with experimental RDFs across the full pressure range, even beyond the first peak. Both the first and second peaks of the TIP5P O···H RDF are consistently about 0.2 shorter than the experimental results at 423 K.

Molecular Interactions. It has been speculated that the tetrahedral network in materials such as water and liquid SiO_2 plays a critical role in their anomalous behaviors.[36] Both liquid water and SiO_2 display density maxima, with the latter at 1500 °C. The tetrahedral network in water is maintained by the hydrogen bonds. The improvement in calculated properties on moving from TIP3P to TIP4P and TIP5P is attributed to better description of water−water interactions, possibly leading to enhancement of tetrahedral structure in the liquid. One characterization of such interactions is the dimer association energy as a function of the dimer flap angle (the angle between the vector connecting the donor and acceptor oxygen atoms, and the vector bisecting the HOH angle of the H-bond acceptor water, as illustrated in Figure 7). It was shown by Mahoney

somewhat less dramatic than that for AMOEBA. The greater change in the AMOEBA RDF in the 3.4 to 4.5 Å region can be attributed to a more rapid diminishment of the ice II state and enhanced ice Ih-like character as the temperature decreases, leading to a density maximum at a slightly higher temperature for AMOEBA.

Radial distribution functions for water under ambient conditions, as well as at various extreme temperatures and pressures, have been derived from neutron scattering experiments by Soper.[35] A direct comparison of the experimental O···O RDF with AMOEBA and TIP5P results is presented in Figure 6(a) through 6(c). The overall agreement between AMOEBA and the experimental RDFs is reasonable, but subtle differences emerge upon closer inspection. The first peak locations in both
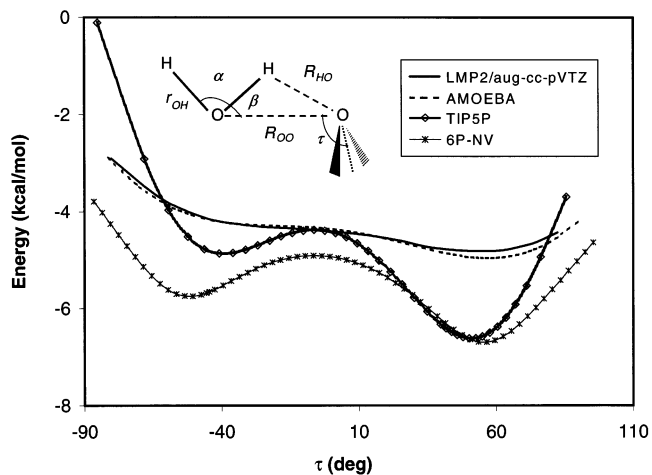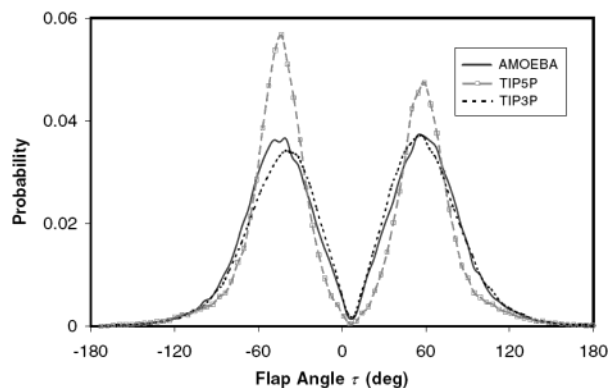
AMOEBA Water Model

J. Phys. Chem. B, Vol. 108, No. 35, 2004 **13433**

Figure 8. Distribution of water dimer flap angle values in simulations of liquid water at ambient temperature and pressure.

and Jorgensen[12] that, unlike the TIP3P and TIP4P water dimers, the TIP5P dimer association energy possessed a double-well dependence on this angle, with the minimum energy angles corresponding more closely to those found in tetrahedral structures. We compare the dimer association energy profile with respect to flap angle for AMOEBA, TIP5P, 6P−NV, and ab initio quantum results at the LMP2/aug-cc-pVQZ level in Figure 7. The 6P−NV potential gives a similar double-well profile to that of TIP5P. However both models yield stronger interactions than found in the ab initio calculations, as required by a nonpolarizable model designed for liquid simulation. The AMOEBA and AMOEBA-v models exhibit nearly indistinguishable energy profiles. A shallow plateau occurs near a flap angle of 40° with the global minimum located at 57°, as also predicted by LMP2/aug-cc-pVTZ calculations. The complete basis set (CBS) MP2 dimer energy at the global minimum is estimated to be 5.0 kcal/mol.[37,38] Another way to examine the orientationally averaged water−water interactions is to look at the second virial coefficients. We have reported previously the AMOEBA second virial coefficients at temperatures between 298 and 773 K. These coefficients, calculated directly from water dimer interactions averaged over all possible orientations at a range of O···O distances, are in excellent agreement with experimental values. The corresponding AMOEBA-v results, not reported here, are very similar to those for AMOEBA. To achieve the liquid density anomaly, it seems necessary for the water dimer to possess an energy minimum for tetrahedral configurations. However, this will cause a nonpolarizable model to overestimate the dimer interaction energy. Unfortunately, the gas-phase dimer interaction does not explain the TMD discrepancy between AMOEBA and AMOEBA-v in the liquid.

Analysis of dynamics trajectories was performed to directly sample the water−water flap angle from liquid simulations at 298 K. The histogram of flap angles, shown in Figure 8, confirms that TIP5P is on average more tetrahedral in the liquid than either TIP3P or the AMOEBA variants. However, the sharp peaks in TIP5P population at tetrahedral flap angles, corresponding to the deep wells observed in the dimer energy profile in Figure 7, indicate enhanced structure beyond that found for the AMOEBA model. Upon investigating the flap angle distributions for AMOEBA between 260 K and 348 K, it is found that peak height increases with decreasing temperature while the most probable flap angle remains essentially constant. The increase in the probability peak also becomes more dramatic at low temperature, indicating a prevalence of tetrahedral structure that leads to the sharp density decrease in the supercooled region.

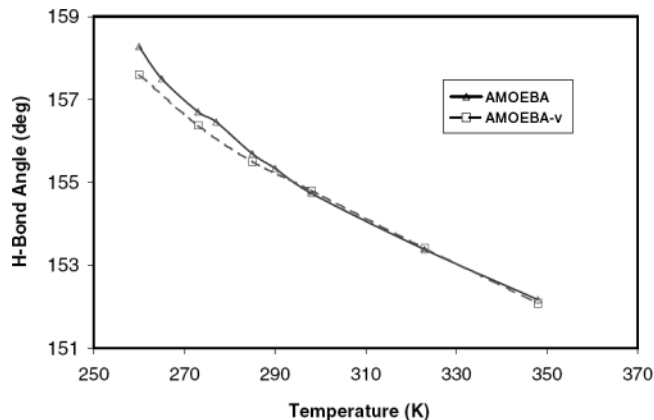The hydrogen bond angle OH···O was conjectured to be critical in the water density anomaly since water has a much

Figure 9. Average hydrogen bond angle in AMOEBA and AMOEBA-v water as a function of temperature.

sharper density maximum transition than liquid SiO_2 with its Si−O−Si angle of about 144°.[36] In Figure 9, the average OH···O angle values are presented for both AMOEBA and AMOEBA-v at room temperature. A maximum O···H distance of 2.9 Å and a maximum OH···O angle of 120° were used as the hydrogen bond criteria. The common trend is that the angle value becomes larger, favoring enhanced tetrahedral networking, as the temperature declines. AMOEBA displays a slightly steeper change than AMOEBA-v at temperatures below 290 K, where the density reaches the maximum for AMOEBA. This is consistent with our earlier observation that the first minimum and second peak of the O···O RDF deform more rapidly for AMOEBA than for AMOEBA-v as the temperature decreases. The smaller average OH···O angle in AMOEBA-v serves to inhibit development of ice Ih-like structure where the hydrogen bonds are closer to linear than in ice II.

An alternative way to analyze the hydrogen bonding structure in a simulation is to compare with experimental magnetic shielding data. The geometries of hydrogen-bonded water dimer structures have been extracted from simulations at a series of temperatures. The magnetic shielding is correlated with dimer geometry by[39]

$$\sigma = A + Br_{OH} + C\alpha + DR_{HO}^{-3} + E\beta \qquad (6)$$

where σ can be either the isotropic average shielding, σ_{ISO}, or the anisotropy, $\Delta\sigma$. The geometric parameters r_{OH}, R_{HO}, α, and β are defined in Figure 7. The values of A through E are constants (different for σ_{ISO} and $\Delta\sigma$) that have been determined from density functional theory by Modig et al.[39] Using these same constants, we have computed σ_{ISO} and $\Delta\sigma$ from the simulation-sampled geometries. The results, shown in Figure 10, are in good agreement with experiment for the average shielding, while the shielding anisotropy of both AMOEBA and AMOEBA-v shows somewhat too weak of a temperature dependence. There is little difference in the overall trends produced by the two models.

Heat of Vaporization and Heat Capacity. The heat of vaporization, ΔH_{vap}, of water at room temperature is one of the data points used in parametrization of the AMOEBA models. Most water potentials, such as TIP4P, TIP4P/FQ, TIP5P, and POL5/T(Q)Z, exhibit a larger temperature dependence for ΔH_{vap} than does real water (see, e.g., Figure 16 in Stern et al.[9] and Figure 12 in Yu et al.[5]). A similar trend is observed for AMOEBA in Figure 11. This temperature dependence is obviously related to the heat capacity C_p. However, the temperature derivative of ΔH_{vap} gives rise to ΔC_p, the difference
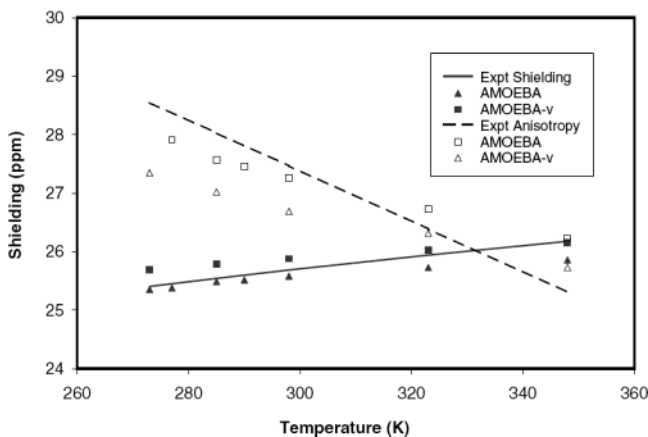
Figure 10. Comparison of the scalar magnetic shielding and anisotropy from AMOEBA water, AMOEBA-v water, and experiment. The solid line and filled points are the average isotropic shielding data. The dashed line and open points are anisotropy data. The lines are derived from experimental measurements.[39] The squares and triangles are AMOEBA and AMOEBA-v results, respectively.
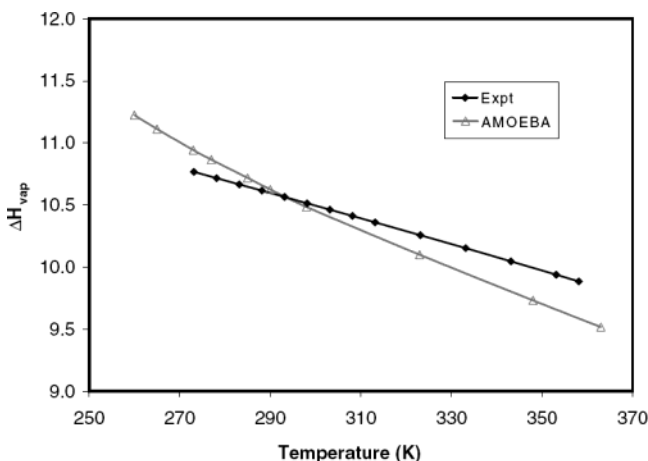

Figure 11. Temperature dependence of the heat of vaporization of water at 1 atm pressure. The experimental data are from Riddick and Bunger.[50]

between the heat capacities of the gas and liquid phases. It can be shown that at room temperature the ΔC_p of water is lower than C_p by 8 cal/mol/K, which is exactly the heat capacity of the gas-phase water (see eq 3, with $3R$ due to kinetic internal energy contribution plus R from the PV term). This difference may explain the discrepancy between the C_p of TIP5P reported by Mahoney and Jorgenson[12] (29 cal/mol/K) and that given by Stern et al.[9] ($\sim$22 cal/mol/K). In this work, the derivative is taken directly from the liquid enthalpy as shown in eq 2.

The behavior of real water is nonclassical. Neither flexible nor rigid molecular mechanics models are fully correct, and corrections must be made in comparing a molecular mechanics-derived heat capacity with experimental values. There has been a suggestion that the quantum correction for a classical rigid water model due to intra- and intermolecular vibrational modes is roughly 2 cal/mol/K.[5] A flexible water model has an intrinsically higher heat capacity than a rigid model, and needs additional correction prior to comparison with experiment. For a rigid water model, the kinetic contribution to the internal energy per molecule is $3RT$ from assignment of $RT/2$ to each degree of freedom. The corresponding value is $9RT/2$ for a flexible water model. If the intramolecular potential energy of a flexible model could be expressed as a harmonic function of generalized coordinates, its contribution to the heat capacity
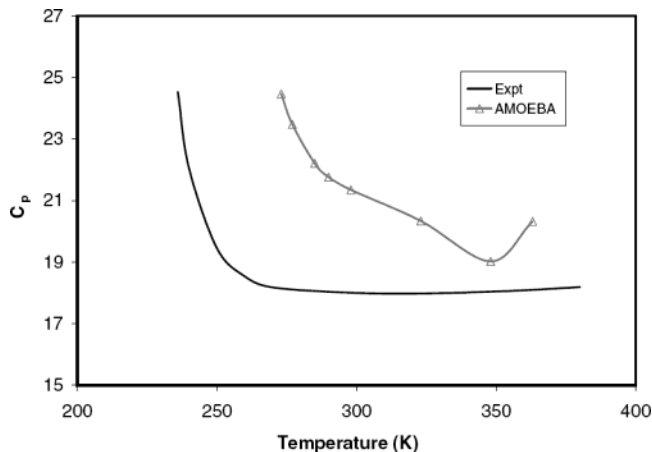

Figure 12. Specific heat capacity of liquid water as a function of temperature. The experimental data are from Angell et al.[51] and from Kell.[24]

would be an additional $3R/2$. Thus, the heat capacity of a flexible model is greater than that of a rigid one by $9R/2 + 3R/2 - 3R = 3R$, or approximately 6 cal/mol/K. Consistent with this estimate, it was shown previously for AMOEBA[13] that C_v is reduced by roughly 7 cal/mol/K when the intramolecular geometry is fixed during simulation. Hence, a total correction of 9 cal/mol/K has been deducted from the AMOEBA results. For example, at room temperature the C_p evaluated from the temperature derivative of the enthalpy is 30.3 cal/mol/K, and a final value of 21.3 cal/mol/K is obtained after correction. In previous work,[13] we reported a C_v calculated from the fluctuation formula to be 28.4 $\pm$ 2.0 cal/mol/K for flexible AMOEBA water. Applying the same correction, this heat capacity estimate becomes 19.4 cal/mol/K. The difference in values obtained from direct differentiation and the fluctuation formula is most likely due to numerical inaccuracy and limited sampling. The statistical uncertainty of enthalpy calculation on average is 50 cal/mol. Thus, the accuracy of C_p estimated by differentiation is roughly $\pm$5 cal/mol/K.

Corrected specific heat capacities over a range of temperatures are plotted in Figure 12. While the heat capacity of ordinary liquids decreases at lower temperatures, water displays a dramatic increase in heat capacity at temperatures below the melting point, and seems to approach a singular state around the supercooling limit temperature of 231 K.[40] Such anomalies have also been observed for the isothermal compressibility and thermal expansion coefficient. The AMOEBA heat capacity exhibits a qualitatively similar anomaly; however, the increase occurs at higher temperatures and is more gradual than for real water. The exaggerated constant pressure heat capacity of AMOEBA water, which may also be expressed as $T(\delta\langle S\rangle/\delta T)_P$ or $\langle dS^2\rangle/k$, is a sign of an overestimation of entropy fluctuations in supercooled water where a tetrahedral network is the dominant local structure.[40]

Self-Diffusion Coefficient. Early fixed-charge water models, such as TIP3P, SPC, and TIP4P, all exhibit much faster dynamics than real water. In contrast, many polarizable models including TIP4P−FQ, DC, and POL5/T(Q)Z have reasonable self-diffusion coefficients, largely due to their explicit inclusion of many-body polarization. Under ambient conditions, TIP5P is reported to have a diffusion coefficient of 2.6×10^{-5} cm^2/s, which is in best agreement among the nonpolarizable models with the experimental value of 2.2×10^{-5} cm^2/s.[41,42] The enhanced tetrahedral structure in the TIP5P water may contribute to this improvement, even though the dipole moment of an isolated TIP5P molecule (2.29 D) is still much less than the
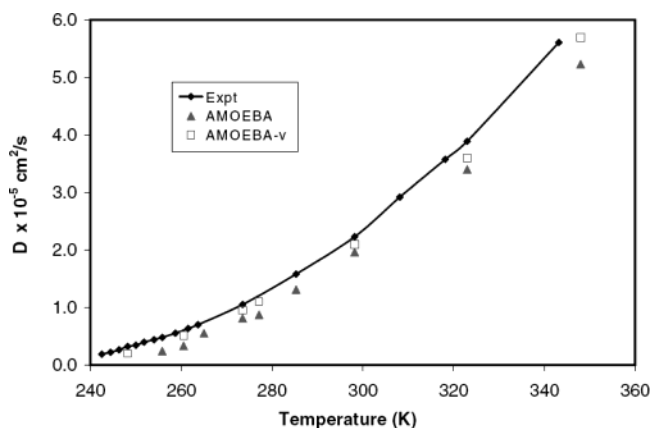
AMOEBA Water Model

J. Phys. Chem. B, Vol. 108, No. 35, 2004 **13435**

Figure 13. Temperature dependence of the self-diffusion coefficient of liquid water. The experimental data are from Mills[41] and from Gillen et al.[42]

commonly accepted value in liquid water (>2.6 D) and the value given by many polarizable models. The temperature dependence of diffusion for AMOEBA and AMOEBA-v water is shown in Figure 13. The AMOEBA-v results are derived from a nanosecond trajectory of a 216-water periodic system, while the AMOEBA values are from a 512-molecule simulation. The diffusion coefficient at 298 K is 1.96×10^{-5} cm^2/s for AMOEBA, consistent with the value of 2.0×10^{-5} cm^2/s previously calculated from an NVT simulation of 216 AMOEBA water molecules. Both AMOEBA and AMOEBA-v results closely follow the experimentally observed diffusion coefficient[41,42] over a full 100-degree temperature span, while AMOEBA-v has slightly better absolute agreement. The difference between simulation and experiment is almost a constant at various temperatures. On average, AMOEBA underestimates the diffusion coefficient by 0.3×10^{-5} cm^2/s. The AMOEBA-v model has a smaller HOH angle in the liquid (101.2°) but a larger average dipole moment (2.85D) than AMOEBA (105.5° and 2.78D). The smaller size of an average AMOEBA-v molecule may contribute to its slightly higher diffusion rate. Overall, the good agreement of the AMOEBA models with experiment is likely due to their improved electrostatic description, especially the inclusion of explicit dipole polarization. It has been suggested that hydrogen bond kinetics in liquid water are notably slowed when explicit polarization is included in a computational model,[43] indicating the necessity of explicit polarization in models that describe water dynamics realistically. Furthermore, it has been suggested that quantum effects, which are missing in classical models, should lead to an increased diffusion constant.[44] This may explain the consistent underestimation of the self-diffusion constant in polarizable models such as AMOEBA, TIP4P/FQ, and POL5/TZ(QZ).

The water self-diffusion constant is known to be relatively insensitive to pressure effects. Its experimental value at room temperature exhibits a maximum around 1000 atm, and decreases monotonically with pressure at high temperatures. Figure 14 presents calculated and experimental diffusion constants as a function of pressure at 298 K and 348 K. Only a few data points have been sampled since the statistical error in the results prohibits drawing any detailed conclusions. As with the temperature dependence, the diffusion coefficients at high pressure are consistently slightly lower than the reported experimental measurements.[45]

Static Dielectric Constant. The static dielectric constant, ϵ_o, is one of the most difficult properties for a water model to reproduce without sacrificing accuracy in other thermodynamic properties, due to its dependence on the fluctuations in the dipole
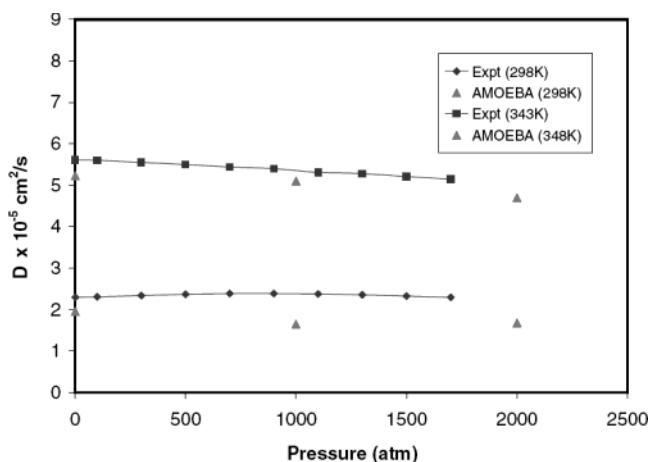

Figure 14. Pressure dependence of the self-diffusion coefficients of liquid water. The experimental data are from Krynicki et al.[45]

TABLE 3: Static Dielectric Constant of Water

		AMOEBA		AMOEBA-v	
temp (K)	expt^a ϵ_o	ϵ_o	$<\mu_{mol}>$	ϵ_o	$<\mu_{mol}>$
273	87.74	87.7 ± 1.5	2.83	104.3 ± 1.6	2.90
298	78.30	81.4 ± 1.4	2.78	88.7 ± 1.6	2.85
323	69.91	66.5 ± 1.2	2.73	82.1 ± 1.5	2.81
348	62.43	57.8 ± 1.4	2.69	67.7 ± 1.2	2.77

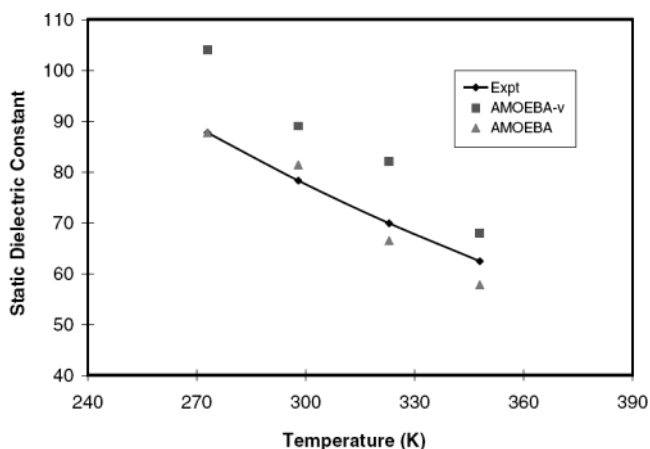^{a} Malmberg and Maryott.[46]

Figure 15. Temperature dependence of the static dielectric constant of liquid water. The experimental data are from Malmberg and Maryott.[46]

and higher order electric moments of the whole system. It also requires lengthy simulations of several nanoseconds in order to achieve a converged value. Using droplet simulations as described above, ϵ_o has been estimated at different temperatures. The results for AMOEBA and AMOEBA-v water are listed in Table 3, and comparison with experiment[46] is made in Figure 15. AMOEBA-v has relatively high dielectric constants from 273 K through 348 K. This is probably due to its consistently larger average molecular dipole moment, which is in turn caused by the smaller HOH bond angle adopted by AMOEBA-v. As we suggested in previous work,[13] the common view that a dipole moment greater than 2.6 D in the liquid would result in an overestimation of the dielectric constant does not appear to hold. In line with our observation, Höchtl et al.[47] have proposed a critical role for average water intramolecular geometry in determining the dielectric constast. According to their argument, the better agreement of AMOEBA's dielectric constant compared to AMOEBA-v can be attributed to the "correct" average

HOH bond angle. Nonetheless, the molecular dipole moment and its fluctuations are obviously directly related to the ϵ_o. The wide range of average molecular dipole moments for water models found in the literature, ranging from 2.2 to 2.8 D, is a direct consequence of the intrinsic electrostatic model, where either no polarization or different polarization treatments are employed. For a given model, artificial enhancement or reduction in the degree of polarization without balancing other components of the potential will undoubtedly undermine the model's overall quality, including the ability to produce the correct dielectric constant.

Conclusions

AMOEBA is an atomic multipole-based model that treats dipole polarization explicitly. The parameters in this water model were derived previously from gas-phase and room-temperature liquid properties, mainly the density and heat of vaporization. It is very encouraging that the AMOEBA model, when extended to simulate water under different thermodynamic conditions, spontaneously reproduces anomalies such the density maximum above the freezing temperature, and the sharp increase in heat capacity in the supercooled region. The quantitative agreement with experimental data ranges from reasonable to excellent for density, radial distribution function, diffusion coefficient, and dielectric constant under various temperature and pressure conditions.

Through comparison of AMOEBA and a variant parametrization, AMOEBA-v, we have demonstrated that much of the anomalous behavior of water is closely related to its hydrogen bonding properties. Internal geometry is shown to be a key factor in determining the properties of a water model because of its correlation with hydrogen bond structure and molecular dipole moment. A flexible model such as AMOEBA is problematic in terms of heat capacity and geometric dependence of electrostatics. A future challenge for empirical potentials therefore lies in the realistic representation of intramolecular interactions, which may inevitably require a nonclassical description. Results presented for computed water radial distribution functions tend to corroborate the view that water possesses a mixture of local tetrahedral-like and denser but less ordered sets of structures. The temperature and pressure dependence of water thermodynamics is governed by the balance between these two structural types. The AMOEBA model is less satisfactory in the pressure dependence of its water density, and behaves similarly to the TIP5P model. It is possible that current generation repulsion-dispersion functional forms need further refinement to address this shortcoming.

Morita has argued from quantum calculations that the molecular polarizability of water in the liquid phase should be smaller by 7−9% than the gas-phase value of 1.44 Å^3, especially along the OH bond direction.[48] The PPC[10] and SWM4-DP[6] models used a further reduction of the gas-phase polarizability (30%) in their development. These adjustments may be necessary if a damping model for short-range polarization is not included. A small reduction in the AMOEBA polarizability might lead to slightly better dynamic properties, however no significant changes in the overall behavior of the model would be expected. It is more consistent at this point to not modify gas-phase dipole moments or use reduced molecular polarizability in the future development of the AMOEBA force field.

If the AMOEBA model is to be applied to larger heterogeneous systems, its computational expense must be compared with that of simpler models. Using the TINKER modeling software, dynamics calculations reported here with the AMOEBA model (using Ewald summation for electrostatics, and a vdW switching window cutoff at 12 Å) are approximately 10 times slower than for TIP5P (using 9-Å truncation for electrostatics and vdW interactions). When the TIP5P model is computed for Particle Mesh Ewald summation and a vdW cutoff scheme equivalent to that for AMOEBA, the CPU time difference is reduced to approximately a factor of 6. Fortunately, many possible CPU-time optimizations are essentially orthogonal to the development of the AMOEBA model itself. For example, a particle-mesh Ewald formulation for multipoles has been developed by Sagui et al.[49] and is in the process of being incorporated into our simulation package. It will greatly improve the speed of the AMOEBA model when applied to large systems, as its computation time scales as $N \log(N)$ with the system size. For a 4000-atom system, the inclusion of atomic dipole and quadrupole moments is reported to lead to only a threefold increase in CPU time compared with simple atomic partial charge-based PME. Subsequent inclusion of induced dipole polarization can be expected to increase the computational cost of large systems to approximately a factor of 5 with respect to fixed atomic charge PME.

Clearly, fixed atomic charge potentials, and other coarse-grained electrostatic representations, provide a sufficient description of water for many applications. However, physically accurate, higher-resolution models are desirable if chemical accuracy is necessary for calculations involving heterogeneous environments. For the case of pure liquid water, explicit polarization offers no immediate advantages in the modeling of certain properties such as density and heat of vaporization. On the other hand, properties such as the self-diffusion coefficient, molecular dipole moment, and other dynamic properties are evidently strongly affected by the presence of secondary effects such as polarization. Equally important is the fact that direct inclusion of many-body polarization leads to less ambiguity in the separation of electrostatic and dispersion components of the potential. The result of the AMOEBA parametrization is a more robust model suitable for addressing the gas-phase dimer and clusters, as well as liquid and solid properties. The better transferability and well-defined physical components of the model make it easily extensible to other small molecules as well as larger, flexible biomacromolecules.

References and Notes

(1) Barnes, P.; Finney, J. L.; Nicholas, J. D.; Quinn, J. E. *Nature* **1979**, *282*, 459.

(2) Stillinger, F. H.; David, C. W. *J. Chem. Phys.* **1978**, *69*, 1473.

(3) Turner, P. J.; David, C. W. *J. Chem. Phys.* **1981**, *74*, 512.

(4) Guillot, B. *J. Mol. Liq.* **2002**, *101*, 219.

(5) Yu, H.; Hansson, T.; van Gunsteren, W. F. *J. Chem. Phys.* **2003**, *118*, 221.

(6) Lamoureux, G.; MacKerell, A. D.; Roux, B. *J. Chem. Phys.* **2003**, *119*, 5185.

(7) Jedlovszky, P.; Vallauri, R. *Mol. Phys.* **1999**, *97*, 1157.

(8) Jedlovszky, P.; Vallauri, R. *J. Chem. Phys.* **2001**, *115*, 3750.

(9) Stern, H. A.; Rittner, F.; Berne, B. J.; Friesner, R. A. *J. Chem. Phys.* **2001**, *115*, 2237.

(10) Svishchev, I. M.; Kusalik, P. G.; Wang, J.; Boyd, R. J. *J. Chem. Phys.* **1996**, *105*, 4742.

(11) Rick, S. W. *J. Chem. Phys.* **2001**, *114*, 2276.

(12) Mahoney, M. W.; Jorgensen, W. L. *J. Chem. Phys.* **2000**, *112*, 8910.

(13) Ren, P.; Ponder, J. W. *J. Phys. Chem. B* **2003**, *107*, 5933.

(14) Ponder, J. W. *TINKER: Software Tools for Molecular Design*; 4.1 ed.; Washington University School of Medicine: Saint Louis, 2003.

AMOEBA Water Model

J. Phys. Chem. B, Vol. 108, No. 35, 2004 **13437**

(15) Berendsen, H. J. C.; Postma, J. P. M.; van Gunsteren, W. F.; DiNola, A.; Haak, J. R. *J. Chem. Phys.* **1984**, *81*, 3684.

(16) Morishita, T. *J. Chem. Phys.* **2000**, *113*, 2976.

(17) Schrödinger, L. L. C. *Jaguar*, Version 4.2; New York, 2002.

(18) Simonson, T. *Chem. Phys. Lett.* **1996**, *250*, 450.

(19) Wallqvist, A.; Ahlström, P.; Karlstrom, G. *J. Phys. Chem.* **1990**, *94*, 1649.

(20) Berendsen, H. J. C.; Postma, J. P. M.; van Gunsteren, W. F.; Hermans, J. Interaction Models for Water in Relation to Protein Hydration. In *Intermolecular Forces*; Pullmann, B., Ed.; D. Reidel Publishing Company: Dordrecht, 1981; p 331.

(21) Jorgensen, W. L.; Chandrasekhar, J.; Madura, J. D.; Impey, R. W.; Klein, M. L. *J. Chem. Phys.* **1983**, *79*, 926.

(22) Berendsen, H. J. C.; Grigera, J. R.; Straatsma, T. P. *J. Phys. Chem.* **1987**, *91*, 6269.

(23) Stillinger, F. H.; Rahman, A. *J. Chem. Phys.* **1974**, *60*, 1545.

(24) Kell, G. S. *J. Chem. Eng. Data* **1975**, *20*, 97.

(25) Nada, H.; van der Eerden, J. P. J. M. *J. Chem. Phys.* **2003**, *118*, 7401.

(26) Jorgensen, W. L.; Jenson, C. *J. Comput. Chem.* **1998**, *19*, 1179.

(27) Burnham, C. J.; Xantheas, S. S. *J. Chem. Phys.* **2002**, *116*, 5115.

(28) Nymand, T. M.; Astrand, P.-O. *J. Phys. Chem. A* **1997**, *101*, 10039.

(29) Ichikawa, K.; Kameda, K.; Yamaguchi, T.; Wakita, H.; Misawa, M. *Mol. Phys.* **1991**, *73*, 79.

(30) Sato, H.; Uematsu, M.; Watanabe, K.; Saul, A.; Wagner, W. *J Phys. Chem. Ref. Data* **1988**, *17*, 1439.

(31) Halgren, T. A. *J. Am. Chem. Soc.* **1992**, *114*, 7827.

(32) Soper, A. K.; Philips, M. G. *Chem. Phys.* **1986**, *107*, 47.

(33) Hura, G.; Sorenson, J. M.; Glaeser, R. M.; Head-Gordon, T. *J. Chem. Phys.* **2000**, *113*, 9140.

(34) Schmid, R. *Monatsh. Chem.* **2001**, *132*, 1295.

(35) Soper, A. K. *Chem. Phys.* **2000**, *258*, 121.

(36) Angell, C. A.; Kanno, H. *Science* **1976**, *193*, 1121.

(37) Klopper, W.; van Duijneveldt-van de Rijdt, J. G. C. M.; van Duijneveldt, F. B. *Phys. Chem. Chem. Phys.* **2000**, *2*, 2227.

(38) Tschumper, G. S.; Leninger, M. L.; Hoffman, B. C.; Valeev, E. F.; Schaefer, H. F., III; Quack, M. *J. Chem. Phys.* **2002**, *116*, 690.

(39) Modig, K.; Pfrommer, B. G.; Halle, B. *Phys. Rev. Lett.* **2003**, *90*, 075502.

(40) Debededetti, P. G.; Stanley, H. E. *Phys. Today* **2003**.

(41) Mills, R. *J. Phys. Chem.* **1973**, *77*, 685.

(42) Gillen, K. T.; Douglass, D. C.; Hoch, M. J. R. *J. Chem. Phys.* **1972**, *57*, 5117.

(43) Xu, H.; Stern, H. A.; Berne, B. J. *J. Phys. Chem. B* **2002**, *106*, 2054.

(44) Lobaugh, J.; Voth, G. A. *J. Chem. Phys.* **1997**, *106*, 2400.

(45) Krynicki, K.; Green, C. D.; Sawyer, D. W. *Faraday Discuss.* **1978**, *66*, 199.

(46) Malmberg, C. G.; Maryott, A. A. *J. Res. Nat. Bur. Stand.* **1956**, *56*, 1.

(47) Höchtl, P.; Boresch, S.; Bitomsky, W.; Steinhauser, O. *J. Chem. Phys.* **1998**, *109*, 4927.

(48) Morita, A. *J. Comput. Chem.* **2002**, *23*, 1466.

(49) Sagui, C.; Pedersen, L. G.; Darden, T. *J. Chem. Phys.* **2004**, *120*, 73.

(50) Riddick, J. A.; Bunger, W. B. *Organic Solvents*, 3rd ed.; Wiley-Interscience: 1970; Vol. II.

(51) Angell, C. A.; Sichina, W. J.; Oguni, M. *J. Phys. Chem.* **1982**, *86*, 998.

(52) Clough, S. A.; Beers, Y.; Klein, G. P.; Rothman, L. S. *J. Chem. Phys.* **1973**, *59*, 2254.

(53) Verhoeven, J.; Dymanus, A. *J. Chem. Phys.* **1970**, *52*, 3222.